Abstracta

Ano XXVI - N. 03

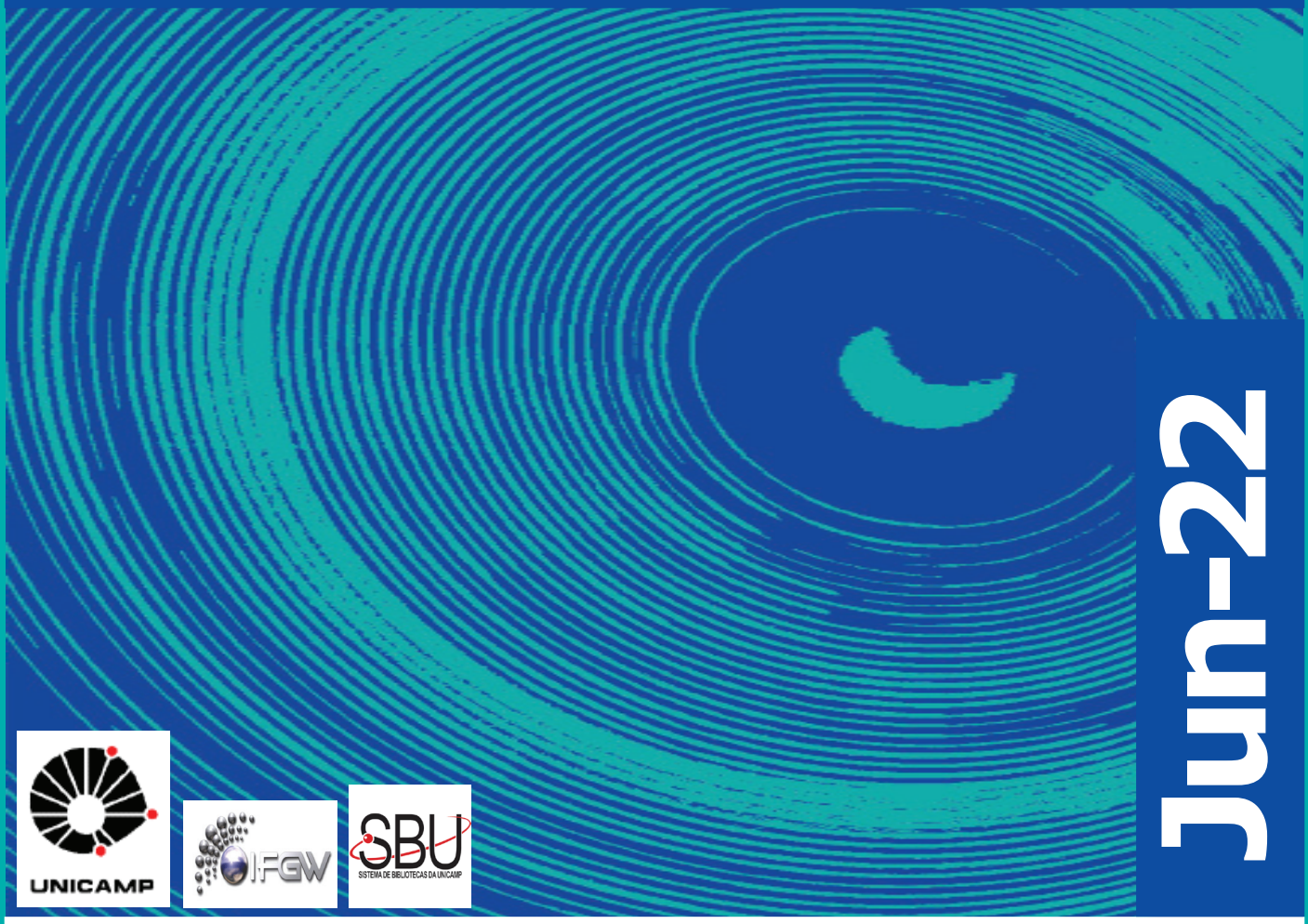

Jun-22

Artigos publicados - P077-2022 à P133-2022

Correções - C003-2022 à C004-2022

Defesas de Dissertações do IFGW - D006-2022 à D012-2022

Defesas de Teses do IFGW - T009-2022 à T010-2022

Artigos publicados

[P077-2022] "A controlled cascade interference"

Alegre, T. P. M.*; Wiederhecker, G. S.*

Nonlinear optical effects enable sophisticated functionalities to generate and manipulate light. The precise control of two distinct nonlinear phenomena in a photonic chip can enhance a key optical nonlinearity that makes single-photon sources more efficient.

NATURE PHYSICS 18[5], 495-496, 2022. DOI: 10.1038/s41567-022-01587-y

[P078-2022] "A direct approach to calculate the temperature dependence of the electronic relaxation time in 2D semiconductors from Boltzmann transport theory"

Tromer, R. M.*; Pereira, L. F. C.; Ferreira, M. S.; Luz, M. G. E. da

We devise a simple heuristic method for obtaining the relaxation time and electrical conductivity dependence on the temperature of carriers in 2D semiconductors. The approach is computationally straightforward. It relies on the BoltzTraP algorithm (from the Boltzmann transport equation), on a direct fitting procedure, and on a proper scaling at a reference temperature. The approach provides a good estimate for the figure of merit ZT, an important characterization of thermoelectricity in materials. We employ our approach to analyze promising 2D systems for thermoelectric applications, namely, nitrogenated holey graphene (NHG), boron-doped NHG, and tungsten disulfide 2D- WS 2. In all these cases, our results agree with computationally expensive calculations available in the literature at a fraction of the computing time.

JOURNAL OF APPLIED PHYSICS 131[11], 115704, 2022. DOI: 10.1063/5.0080938

[P079-2022] "A new calibration method for charm jet identification validated with proton-proton collision events at root s=13 TeV"

Tumasyan, A.; Adam, W.; Andrejkovic, J. W.; **Chinellato, J. A.***; et al. CMS Collaboration

Many measurements at the LHC require efficient identification of heavy-flavour jets, i.e. jets originating from bottom (b) or charm (c) quarks. An overview of the algorithms used to identify c jets is described and a novel method to calibrate them is presented. This new method adjusts the entire distributions of the outputs obtained when the algorithms are applied to jets of different flavours. It is based on an iterative approach exploiting three distinct control regions that are enriched with either b jets, c jets, or light-flavour and gluon jets. Results are presented in the form of correction factors evaluated using proton-proton collision data with an integrated luminosity of 41.5 fb(-1) at root s = 13 TeV, collected by the CMS experiment in 2017. The closure of the method is tested by applying the measured correction factors on simulated data sets and checking the agreement between the adjusted simulation and collision data. Furthermore, a validation is performed by testing the method on pseudodata, which emulate various mismodelling conditions. The calibrated results enable the use of the full distributions of heavy-flavour identification algorithm outputs, e.g. as inputs to machine-learning models. Thus, they are expected to increase the sensitivity of future physics analyses.

JOURNAL OF INSTRUMENTATION 17[3], P03014, 2022. DOI: 10.1088/1748-0221/17/03/P03014

[P080-2022] "Analysis of Cosmogenic Neutron Characteristics and the Pulses Counting Rate Using ASD, LSD, and LVD Scintillation Detectors"

Agafonova, N. Y.; Aglietta, M.; Antonioli, P.; Ashikhmin, V. V.; Bari, G.; Bruno, G.; Dobrynina, E. A.; Enikeev, R., I; Fulgione, W.; Galeotti, P.; Garbinid, M.; Ghia, P. L.; Giust, P.; **Kemp, E.***; Malgin, A. S.; Molinario, A.; Persiani, R.; Pless, I. A.; Ryazhskaya, G.; Sartorelli, G.; Shakiryanova, I. R.; Selvi, M.; Trinchero, G. C.; Vigorito, C. F.; Yakushev, V. F.; Zichichi, A.

Experimental data obtained using three scintillation detectors are analyzed. The characteristics of cosmogenic neutrons in underground experiments their analytic dependences are considered. The behavior of background counting rate for the LVD detector for two measuring thresholds (0.5 and 5 MeV) are discussed.

JOURNAL OF EXPERIMENTAL AND THEORETICAL PHYSICS 134[4], SI, 449-458, 2022. DOI: 10.1134/S1063776122040124

[P081-2022] "Assessing the best time interval between doses in a two-dose vaccination regimen to reduce the number of deaths in an ongoing epidemic of SARS-CoV-2"

Ferreira, L. S.; Canton, O.; Silva, R. L. P. da; Poloni, S.; Sudbrack, V.; Borges, M. E.; Franco, C.; **Marquitti, F. M. D.***; Moraes, J. C. de; Veras, M. A. D. M.; Kraenkel, R. A.; Coutinho, R. M.

The SARS-CoV-2 pandemic is a major concern all over the world and, as vaccines became available at the end of 2020, optimal vaccination strategies were subjected to intense investigation. Considering their critical role in reducing disease burden, the increasing demand outpacing production, and that most currently approved vaccines follow a two-dose regimen, the cost-effectiveness of delaying the second dose to increment the coverage of the population receiving the first dose is often debated. Finding the best solution is complex due to the trade-off between vaccinating more people with lower level of protection and guaranteeing higher protection to a fewer number of individuals. Here we present a novel extended age-structured SEIR mathematical model that includes a two-dose vaccination schedule with a between-doses delay modelled through delay differential equations and linear optimization of vaccination rates. By maintaining the minimum stock of vaccines under a given production rate, we evaluate the dose interval that minimizes the number of deaths. We found that the best strategy depends on an interplay between the vaccine production rate and the relative efficacy of the first dose. In the scenario of low first-dose efficacy, it is always better to vaccinate the second dose as soon as possible, while for high first-dose efficacy, the best strategy of time window depends on the production rate and also on second-dose efficacy provided by each type of vaccine. We also found that the rate of spread of the infection does not affect significantly the thresholds of the best window, but is an important factor in the absolute number of total deaths. These conclusions point to the need to carefully take into account both vaccine characteristics and roll-out speed to optimize the outcome of vaccination strategies.

PLOS COMPUTATIONAL BIOLOGY 18[3], e1009978, 2022. DOI: 10.1371/journal.pcbi.1009978

[P082-2022] "Auxetic properties of a newly proposed gamma-graphyne-like material"

Paupitz, R.; Silva, T. J. da; Caldas, M. J.; **Galvao, D. S.*; Fonseca, A. F.***

A new auxetic (negative Poisson's ratio values) structure based on a gamma-graphyne structure, here named A gamma G structure, is proposed. The A gamma G structural/mechanical and electronic properties, as well as its thermal stability, were investigated using classical reactive and quantum molecular dynamics simulations. A gamma G is shown to have a bandgap larger than 1.6 eV and be thermally stable at a large range of temperatures. The classical and quantum results validate that the A gamma G is auxetic, both when isolated (vacuum) and when deposited on a copper substrate. We believe that this is the densest auxetic structure belonging to the graphyne-like families.

CHEMICAL PHYSICS LETTERS 787, 139220, 2022. DOI: 10.1016/j.cplett.2021.139220

[P083-2022] "Boundary conditions for isolated asymptotically anti-de Sitter spacetimes"

Oliveira, C. C. de*; Mosna, R. A.; Pitelli, J. P. M.

We revisit the propagation of classical scalar fields in a spacetime, which is asymptotically anti-de Sitter. The lack of global hyperbolicity of the underlying background gives rise to an ambiguity in the dynamical evolution of solutions of the wave equation, requiring the prescription of extra boundary conditions at the conformal infinity to be fixed. We show that the only boundary conditions that are compatible with the hypothesis that the system is isolated, as defined by the (improved) energy-momentum tensor, are of Dirichlet and Neumann types.

JOURNAL OF MATHEMATICAL PHYSICS 63[4], 042501, 2022. DOI: 10.1063/5.0078118

[P084-2022] "Comprehending Cardiac Dysfunction by Oxidative Stress: Untargeted Metabolomics of In Vitro Samples"

Amaral, A. G.; Moretto, I. A.; Zandonadi, F.D. da S.; Zamora-Obando, H. R.; Rocha, I.; Sussulini, A.; **Thomaz, A. A. de***; Oliveira, R. V.; Santos, A. M. dos; Simionato, A. V. C.

Cardiovascular diseases (CVDs) are noncommunicable diseases known for their complex etiology and high mortality rate. Oxidative stress (OS), a condition in which the release of free radical exceeds endogenous antioxidant capacity, is pivotal in CVC, such as myocardial infarction, ischemia/reperfusion, and heart failure. Due to the lack of information about the implications of OS on cardiovascular conditions, several methodologies have been applied to investigate the causes and consequences, and to find new ways of diagnosis and treatment as well. In the present study, cardiac dysfunction was evaluated by analyzing cells' alterations with untargeted metabolomics, after simulation of an oxidative stress condition using hydrogen peroxide (H2O2) in H9c2 myocytes. Optimizations of H2O2 concentration, cell exposure, and cell recovery times were performed through MTT assays. Intracellular metabolites were analyzed right after the oxidative stress (oxidative stress group) and after 48 h of cell recovery (recovery group) by ultra-high-performance liquid chromatography coupled to mass spectrometry (UHPLC-MS) in positive and negative ESI ionization mode. Significant alterations were found in pathways such as "alanine, aspartate and glutamate metabolism", "glycolysis", and "glutathione metabolism", mostly with increased metabolites (upregulated). Furthermore, our results indicated that the LC-MS method is effective for studying metabolism in cardiomyocytes and generated excellent fit ((RY)-Y-2 > 0.987) and predictability (Q(2) > 0.84) values.

FRONTIERS IN CHEMISTRY 10, 836478, 2022. DOI: 10.3389/fchem.2022.836478

[P085-2022] "Coverage-dependent study of nickel tetraphenyl-porphyrin on Au(332) and Au(788)"

Fatayer, S.; Prieto, M. J.; **Landers, R.*; Siervo, A. de***

The coverage-dependent self-assembly of Nickel-tetraphenyl porphyins on Gold vicinal surfaces was studied by scanning tunneling microscopy. On Au(788) the molecular self-assembly is square-shaped, following the molecular symmetry. On Au(332) the molecules nucleate in a parallelogram lattice for monolayer coverage and in a squared lattice for multilayer coverage. Depending on the vicinal surface the molecules adopt either a saddle shaped or a more planar conformation. The experiments demonstrate that crystallographic direction, terrace sizes and coverage are important in establishing different assembly geometries.

SURFACE SCIENCE 723, 122105, 2022. DOI: 10.1016/j.susc.2022.122105

[P086-2022] "Design and implementation of a device based on an off-axis parabolic mirror to perform luminescence experiments in a scanning tunneling microscope"

Roman, R. J. P.*; Auad, Y.*; Grasso, L.*; Padilha, L. A.*; Alvarez, F.*; Barcelos, I. D.; Kociak, M.; **Zagonel, L. F.***

We present the design, implementation, and illustrative results of a light collection/injection strategy based on an off-axis parabolic mirror collector for a low-temperature Scanning Tunneling Microscope (STM). This device allows us to perform STM induced Light Emission (STM-LE) and Cathodoluminescence (STM-CL) experiments and in situ Photoluminescence (PL) and Raman spectroscopy as complementary techniques. Considering the etendue conservation and using an off-axis parabolic mirror, it is possible to design a light collection and injection system that displays 72% of collection efficiency (considering the hemisphere above the sample surface) while maintaining high spectral resolution and minimizing signal loss. The performance of the STM is tested by atomically resolved images and scanning tunneling spectroscopy results on standard sample surfaces. The capabilities of our system are demonstrated by performing STM-LE on metallic surfaces and two-dimensional semiconducting samples, observing both plasmonic and excitonic emissions. In addition, we carried out in situ PL measurements on semiconducting monolayers and quantum dots and in situ Raman on graphite and hexagonal boron nitride (h-BN) samples. Additionally, STM-CL and PL were obtained on monolayer h-BN gathering luminescence spectra that are typically associated with intragap states related to carbon defects. The results show that the flexible and efficient light injection and collection device based on an off-axis parabolic mirror is a powerful tool to study several types of nanostructures with multiple spectroscopic techniques in correlation with their morphology at the atomic scale and electronic structure.

REVIEW OF SCIENTIFIC INSTRUMENTS 93[4], 043704, 2022. DOI: 10.1063/5.0078423

[P087-2022] "Developed and characterization of nanostructured lipid carriers containing food-grade interesterified lipid phase for food application"

Silva, M. G. da; Godoi, K. R. R. de; Gigante, M. L.; **Cardoso, L. P.*;** Ribeiro, A. P. B.

The main objectives of our work were to produce new nanostructured lipid carriers (NLCs) from interesterified and simple lipid phases and to study the influence of lipid composition on the physical characteristics and stability of NLCs. We used conventional oils and fats already used in lipid-based foods, in addition to soy lecithin as a natural emulsifier.

The NLCs were formulated using as lipid phase, simple and interesterified blends composed of soybean oil as liquid lipid and fully hydrogenated oils from palm, soybean, microalgae, and crambe as solid lipids. NLCs were produced using high--pressure homogenization. NLCs were influenced by chemical interesterification and by the composition of the solid lipid used, mainly in relation to the fatty acid chain size. NLC formulations developed with a simple lipid phase were 256-323 nm (d(32)) in size, with zeta potential values ranging from -36.93 to -42.87 mV after 60 days of storage. NLCs developed with the interesterified lipid phase were 250-288 nm (d(32)) in size, with zeta potential values ranging from -40.17 to -44.20 mV after 60 days of storage. NLCs produced with saturated fatty acids with larger chain sizes showed larger particle sizes but showed less variation in this parameter over storage. Interesterification reduced the melting temperature of NLCs, indicating decreased crystallinity and a less organized structure. Moreover, interesterification favored crystals in the beta' form, which is a positive characteristic for incorporating bioactive compounds. Thus, the systems developed in this study are innovative, mainly in terms of the composition of the NLCs, and have good potential for food applications.

FOOD RESEARCH INTERNATIONAL 155, 111119, 2022. DOI: 10.1016/j.foodres.2022.111119

[P088-2022] "Devising Bone Molecular Models at the Nanoscale: From Usual Mineralized Collagen Fibrils to the First Bone Fibers Including Hydroxyapatite in the Extra-Fibrillar Volume"

Alcantara, A. C. S.; **Felix, L. C.*; Galvao, D. S.*;** Sollero, P.; Skaf, M. S.

At the molecular scale, bone is mainly constituted of type--I collagen, hydroxyapatite, and water. Different fractions of these constituents compose different composite materials that exhibit different mechanical properties at the nanoscale, where the bone is characterized as a fiber, i.e., a bundle of mineralized collagen fibrils surrounded by water and hydroxyapatite in the extra-fibrillar volume. The literature presents only models that resemble mineralized collagen fibrils, including hydroxyapatite in the intra-fibrillar volume only, and lacks a detailed prescription on how to devise such models. Here, we present all-atom bone molecular models at the nanoscale, which, differently from previous bone models, include hydroxyapatite both in the intra-fibrillar volume and in the extra-fibrillar volume, resembling fibers in bones. Our main goal is to provide a detailed prescription on how to devise such models with different fractions of the constituents, and for that reason, we have made step-by-step scripts and files for reproducing these models available. To validate the models, we assessed their elastic properties by performing molecular dynamics simulations that resemble tensile tests, and compared the computed values against the literature (both experimental and computational results). Our results corroborate previous findings, as Young's Modulus values increase with higher fractions of hydroxyapatite, revealing all-atom bone models that include hydroxyapatite in both the intra-fibrillar volume and in the extra-fibrillar volume as a path towards realistic bone modeling at the nanoscale.

MATERIALS 15[6], 2274, 2022. DOI: 10.3390/ma15062274

[P089-2022] "Direct observation of the dead-cone effect in quantum chromodynamics"

Acharya, S.; Adamova, D.; Adler, A.; **Chinellato, D. D.*; Guardiano, G. G.*; Jahnke, C.*; Takahashi, J.***; et al. ALICE Collaboration

In particle collider experiments, elementary particle interactions with large momentum transfer produce quarks and gluons (known as partons) whose evolution is governed by the strong force, as described by the theory of quantum chromodynamics (QCD)(1). These partons subsequently emit further partons in a process that can be described as a parton shower(2), which culminates in the formation of detectable hadrons. Studying the pattern of the parton shower is one of the key experimental tools for testing QCD. This pattern is expected to depend on the mass of the initiating parton, through a phenomenon known as the dead-cone effect, which predicts a suppression of the gluon spectrum emitted by a heavy quark of mass m(Q) and energy E, within a cone of angular size m(Q)/E around the emitter(3). Previously, a direct observation of the dead-cone effect in QCD had not been possible, owing to the challenge of reconstructing the cascading quarks and gluons from the experimentally accessible hadrons. We report the direct observation of the QCD dead cone by using new iterative declustering techniques(4,5) to reconstruct the parton shower of charm quarks. This result confirms a fundamental feature of QCD. Furthermore, the measurement of a dead-cone angle constitutes a direct experimental observation of the non-zero mass of the charm quark, which is a fundamental constant in the standard model of particle physics.

NATURE 605[7910], 440-+, 2022. DOI: 10.1038/s41586-022-04572-w

[P090-2022] "Effects of Systemic Physiology on Mapping Resting-State Networks Using Functional Near-Infrared Spectroscopy"

Abdalmalak, A.; **Novi, S. L.***; Kazazian, K.; Norton, L.; Benaglia, T.; Slessarev, M.; Debicki, D. B.; St Lawrence, K.; **Mesquita, R. C.***; Owen, A. M.

Resting-state functional connectivity (rsFC) has gained popularity mainly due to its simplicity and potential for providing insights into various brain disorders. In this vein, functional near-infrared spectroscopy (fNIRS) is an attractive choice due to its portability, flexibility, and low cost, allowing for bedside imaging of brain function. While promising, fNIRS suffers from non-neural signal contaminations (i.e., systemic physiological noise), which can increase correlation across fNIRS channels, leading to spurious rsFC networks. In the present work, we hypothesized that additional measurements with short channels, heart rate, mean arterial pressure, and end--tidal CO2 could provide a better understanding of the effects of systemic physiology on fNIRS-based resting-state networks. To test our hypothesis, we acquired 12 min of resting-state data from 10 healthy participants. Unlike previous studies, we investigated the efficacy of different pre-processing approaches in extracting resting-state networks. Our results are in agreement with previous studies and reinforce the fact that systemic physiology can overestimate rsFC. We expanded on previous work by showing that removal of systemic physiology decreases intra- and inter-subject variability, increasing the ability to detect neural changes in rsFC across groups and over longitudinal studies. Our results show that by removing systemic physiology, fNIRS can reproduce resting-state networks often reported with functional magnetic resonance imaging (fMRI). Finally, the present work details the effects of systemic physiology and outlines how to remove (or at least ameliorate) their contributions to fNIRS signals acquired at rest.

FRONTIERS IN NEUROSCIENCE 16, 803297, 2022. DOI: 10.3389/fnins.2022.803297

[P091-2022] "Electrical transport mechanisms of Neodymium-doped rare-earth semiconductors"

Vaz, I. C. F.; Macchi, C. E.; Somoza, A.; Rocha, L. S. R.; Longo, E.; **Cabral, L.*; Silva, E. Z. da***; Simoes, A. Z.; Zonta, G.; Malagu, C.; Desimone, P. M.; Ponce, M. A.; Moura, F.

This study reports the electrical properties of Nd-doped cerium oxide (CeO2) films synthesized by microwave assisted hydrothermal using a two-point probe technique. Positron annihilation lifetime spectroscopy studies evidenced that, as the Nd content rises, a structural disorder occurs. This is caused by an increase in oxygen vacancies surrounded with Nd (defective clusters), with the mean lifetime components ranging between 290 and 300 ps. Particle size estimation showed values from 8.6 to 28.9 nm. Along with the increase of neodymium impurities, also the conductivity increases, due to the hopping conduction mechanism between defective species. This gives rise to a response time of only 6 s, turning these materials candidates to realize gas sensor devices. Ab initio investigations showed that the improved electric conduction is boosted mostly by the reduced Nd2+ than the Ce3+, where the oxygen vacancies play a fundamental role.

JOURNAL OF MATERIALS SCIENCE-MATERIALS IN ELECTRONICS 33[15], 11632-11649, 2022. DOI: 10.1007/s10854-022-08098-9

[P092-2022] "Enhanced magnetism and suppressed magnetoelastic coupling induced by electron doping in Ca1-x Y x MnReO6"

Cavichini, A. S.; Orlando, M. T. D.; Fantini, M. C. A.; **Tartaglia, R.*; Galdino, C. W.***; Damay, F.; Porcher, F.; **Granado, E.***

The Ca2MnReO6 double perovskite is a spin-orbit-assisted Mott insulator with exotic magnetic properties, including a largely non-collinear Mn2+ spin arrangement and nearly orthogonal coupling between such spins and the much smaller Re 5d magnetic moments. Here, the electron-doped compound Ca1-x Y x MnReO6 (x = 0.1, 0.2 and 0.3) is reported and a detailed investigation is conducted for x = 0.3. Neutron and x-ray powder diffraction confirm that nearly full chemical order is maintained at the Mn and Re sites under the Y substitution at the Ca site. X-ray absorption measurements and an analysis of the Mn-O/Re-O bond distances show that the Mn oxidation state remains stable at +2 whereas Re is reduced upon doping. The electron doping increases the magnetic ordering temperature from T (c) = 121 to 150 K and also enhances significantly the ferromagnetic component of the Mn spins at the expense of the antiferromagnetic component at the base temperature (T = 3 K). The lattice parameter anomalies at T (c) observed in the parent compound are suppressed by the electron doping. The possible reasons for the enhanced magnetism and the suppressed magnetoelastic coupling in Ca1.7Y0.3MnReO6 are discussed.

JOURNAL OF PHYSICS-CONDENSED MATTER 34[24], 245803, 2022. DOI: 10.1088/1361-648X/ac61b5

[P093-2022] "Enhancement in magnetization of two-dimensional cobalt telluride and its magnetic field-assisted photocatalytic activity"

Negedu, S. D.; **Tromer, R.***; Siddique, S.; Woellner, C. F.; Olu, F. E.; Palit, M.; Roy, A. K.; Pandey, P.; **Galvao, D. S.***; Kumbhakar, P.; Tiwary, C. S.

Magnetism in semiconductor two-dimensional (2D) materials is gaining popularity due to its potential applications in memory devices, sensors, spintronics, and biomedical applications. Here, 2D cobalt telluride (CoTe) has been synthesized from its bulk crystals using a simple and scalable liquid-phase exfoliation method. The ultrathin CoTe shows similar to 400 times enhancement in its magnetic saturation values compared to the bulk form. The UV-Vis absorption spectra reveal superior absorption in the high-energy region, suggesting a semiconducting nature. Furthermore, we explain the bandgap and origin of high magnetic behavior by density functional theory (DFT) calculations. The 2D CoTe shows a larger magnetism compared to bulk CoTe due to the reduced coordination number of the surface atoms, shape anisotropy, and surface charge effect. Additionally, the semiconducting nature and surface charges are fruitfully utilized for degradation of different toxic dyes under magnetic field and visible light irradiation. Therefore, atomically thin magnetic CoTe can give a new perspective to the separation of charge carriers.

APPLIED PHYSICS A-MATERIALS SCIENCE & PROCESSING 128[5], 379, 2022. DOI: 10.1007/s00339-022-05425-z

[P094-2022] "Experimental cross sections for water ionization due to the impact of light ions-A review"

Bernal, M. A.*; Liendo, J. A.; Incerti, S.; Francis, Z.; Tran, H. N.

This work is a short review on the experimental cross sections for water ionization due to the impact of light ions (Z < 6), including related processes such as electron capture and water molecule fragmentation. These cross sections are crucial in studies dealing with the biological effects produced by the impact of ions on living beings. Physical interpretations of the experimental results are also provided.

NUCLEAR INSTRUMENTS & METHODS IN PHYSICS RESEARCH SECTION B-BEAM INTERACTIONS WITH MATERIALS AND ATOMS 517, 6-15, 2022. DOI: 10.1016/j.nimb.2022.01.015

[P095-2022] "From quantum speed limits to energy-efficient quantum gates"

Aifer, M.; **Deffner, S.***

While recent breakthroughs in quantum computing promise the nascence of the quantum information age, quantum states remain delicate to control. Moreover, the required energy budget for large scale quantum applications has only sparely been considered. Addressing either of these issues necessitates a careful study of the most energetically efficient implementation of elementary quantum operations. In the present analysis, we show that this optimal control problem can be solved within the powerful framework of quantum speed limits. To this end, we derive state-independent lower bounds on the energetic cost, from which we find the universally optimal implementation of unitary quantum gates, for both single and N-qubit operations.

NEW JOURNAL OF PHYSICS 24[5], 055002, 2022. DOI: 10.1088/1367-2630/ac6821

[P096-2022] "Half-integer anomalous currents in 2D materials from a QFT viewpoint"

Dudal, D.; **Matusalem, F.*;** Mizher, A. J.; Rocha, A. R.; Villavicencio, C.

Charge carriers in Dirac/Weyl semi-metals exhibit a relativistic-like behavior. In this work we propose a novel type of intrinsic half-integer Quantum Hall effect in 2D materials, thereby also offering a topological protection mechanism for the current. Its existence is rooted in the 2D parity anomaly, without any need for a perpendicular magnetic field. We conjecture that it may occur in disturbed honeycomb lattices where both spin degeneracy and time reversal symmetry are broken.

These configurations harbor two distinct gap-opening mechanisms that, when occurring simultaneously, drive slightly different gaps in each valley, causing a net anomalous conductivity when the chemical potential is tuned to be between the distinct gaps. Some examples of promising material setups that fulfill the prerequisites of our proposal are also listed to motivate looking for the effect at the numerical and experimental level.

SCIENTIFIC REPORTS 12[1], 5439, 2022. DOI: 10.1038/s41598-022-09483-4

[P097-2022] "Improving Quantitative EDS Chemical Analysis of Alloy Nanoparticles by PCA Denoising: Part II. Uncertainty Intervals"

Moreira, M.*; Hillenkamp, M.*; Divitini, G.; Tizei, L. H. G.; Ducati, C.; **Cotta, M. A.*; Rodrigues, V.*; Ugarte, D.***

Analytical studies of nanoparticles (NPs) are frequently based on huge datasets derived from hyperspectral images acquired using scanning transmission electron microscopy. These large datasets require machine learning computational tools to reduce dimensionality and extract relevant information. Principal component analysis (PCA) is a commonly used procedure to reconstruct information and generate a denoised dataset; however, several open questions remain regarding the accuracy and precision of reconstructions. Here, we use experiments and simulations to test the effect of PCA processing on data obtained from AuAg alloy NPs a few nanometers wide with different compositions. This study aims to address the reliability of chemical quantification after PCA processing. Our results show that the PCA treatment mitigates the contribution of Poisson noise and leads to better quantification, indicating that denoised results may be reliable from the point of view of both uncertainty and accuracy for properly planned experiments. However, the initial data need to be of sufficient quality: these results can only be obtained if the signal-to--noise ratio of input data exceeds a minimal value to avoid the occurrence of random noise bias in the PCA reconstructions.

MICROSCOPY AND MICROANALYSIS, PII S1431927622000551, 2022. DOI: 10.1017/S1431927622000551

[P098-2022] "Investigating charm production and fragmentation via azimuthal correlations of prompt D mesons with charged particles in pp collisions at root s=13 TeV"

Acharya, S.; Adamova, D.; Adler, A.; **Chinellato, D. D.*; Guardiano, G. G.*; Jahnke, C.*; Takahashi, J.***; et al. ALICE Collaboration

Angular correlations of heavy-flavour and charged particles in high-energy proton-proton collisions are sensitive to the production mechanisms of heavy quarks and to their fragmentation as well as hadronisation processes. The measurement of the azimuthal-correlation function of prompt D mesons with charged particles in proton-proton collisions at a centre-of--mass energy of root s = 13 TeV with the ALICE detector is reported, considering D-0, D+, and D*(+) mesons in the transverse-momentum interval 3 < p(T) < 36 GeV/c at midrapidity (vertical bar y vertical bar < 0.5), and charged particles with p(T) > 0.3 GeV/c and pseudorapidity vertical bar eta vertical bar < 0.8. This measurement has an improved precision and provides an extended transverse-momentum coverage compared to previous ALICE measurements at lower energies. The study is also performed as a function of the charged-particle multiplicity, showing no modifications of the correlation function with multiplicity within uncertainties. The properties and the transverse-momentum evolution of the near- and awayside correlation peaks are studied and compared with predictions from various Monte Carlo event generators. Among those considered, PYTHIA8 and POWHEG+PYTHIA8 provide the best description of the measured observables. The obtained results can provide guidance on tuning the generators.

EUROPEAN PHYSICAL JOURNAL C 82[4], 335, 2022. DOI: 10.1140/epjc/s10052-022-10267-3

[P099-2022] "Large-Area Nanopillar Arrays by Glancing Angle Deposition with Tailored Magnetic Properties"

Navarro, E.; Gonzalez, M. U.; **Beron, F.***; Tejo, F.; Escrig, J.; Garcia-Martin, J. M.

Ferromagnetic films down to thicknesses of tens of nanometers and composed by polycrystalline Fe and Fe2O3 nanopillars are grown in large areas by glancing angle deposition with magnetron sputtering (MS-GLAD). The morphological features of these films strongly depend on the growth conditions. Vertical or tilted nanopillars have been fabricated depending on whether the substrate is kept rotating azimuthally during deposition or not, respectively. The magnetic properties of these nanopillars films, such as hysteresis loops squareness, adjustable switching fields, magnetic anisotropy and coercivity, can be tuned with the specific morphology. In particular, the growth performed through a collimator mask mounted onto a not rotating azimuthally substrate produces almost isolated well-defined tilted nanopillars that exhibit a magnetic hardening. The first-order reversal curves diagrams and micromagnetic simulations revealed that a growth-induced uniaxial anisotropy, associated with an anisotropic surface morphology produced by the glancing angle deposition in the direction perpendicular to the atomic flux, plays an important role in the observed magnetic signatures. These results demonstrate the potential of the MS-GLAD method to fabricate nanostructured films in large area with tailored structural and magnetic properties for technological applications.

NANOMATERIALS 12[7], 1186, 2022. DOI: 10.3390/nano12071186

[P100-2022] "Machine learning for sensing with a multimode exposed core fiber specklegram sensor"

Smith, D. L.; Nguyen, L. V.; Ottaway, D. J.; **Cabral, T. D.***; Fujiwara, E.; **Cordeiro, C. M. B.***; Warren-Smith, S. C.

Fiber specklegram sensors (FSSs) traditionally use statistical methods to analyze specklegrams obtained from fibers for sensing purposes, but can suffer from limitations such as vulnerability to noise and lack of dynamic range. In this paper we demonstrate that deep learning improves the analysis of specklegrams for sensing, which we show here for both air temperature and water immersion length measurements. 'Pwo deep neural networks (DNNs); a convolutional neural network and a multi-layer perceptron network, are used and compared to a traditional correlation technique on data obtained from a multimode fiber exposed-core fiber. The ability for the DNNs to be trained against a random noise source such as specklegram translations is also demonstrated.

OPTICS EXPRESS 30[7], 10443-10455, 2022. DOI: 10.1364/OE.443932

[P101-2022] "Magnetic and electronic properties of the RECu4Al8 (RE = Tb, Dy, Ho, and Er) intermetallic compounds"

Mercena, S. G.*; Melo, A. T.*; Lima, A. F.*

Spin density functional theory calculations were employed to study some of the magnetic and electronic properties of the RECu4Al8 (RE = Tb, Dy, Ho, and Er) intermetallic compounds in their tetragonal crystal structure and their collinear antiferromagnetic state. The exchange and correlation electronic effects were treated by both a generalized gradient approximation (GGA) in its recently revised version for solids (GGA-PBEsol), and the addition of the effective Hubbard U term (GGA-PBEsol + U-eff) in the RE 4f states. Based on these methodologies, the total magnetic moment of the RE atoms and their spin and orbital contributions were determined. The total magnetic moment calculated with GGA + PBEsol (U-eff = 0.0 eV) agreed with the experimental data, except for the TbCu4Al8 system, in which the addition of the U(eff)term was needed for a better description. Using GGA + PBEsol, the magnetocrystalline anisotropy energy (MAE), easiest magnetization axis (EMA), exchange splitting of the RE 4f states (delta(ex)), and the electronic specific heat coefficients (gamma) of the four compounds were determined. The values of the MAE found for TbCu4Al8, DyCu4Al8, HoCu4Al8, and ErCu4Al8 were 3.13, 9.11, 26.93, and 17.41 meV/f.u., respectively. The EMA for TbCu4Al8, DyCu4Al8, and HoCu4Al8 was found to be [111], while for ErCu4Al8 it was [001]. The values of delta(ex) were equal to 4.3, 3.6, 2.8, and 1.9 eV for TbCu4Al8, DyCu4Al8, HoCu4Al8, and ErCu4Al8, respectively.

INTERMETALLICS 143, 107474, 2022. DOI: 10.1016/j.intermet.2022.107474

[P102-2022] "Measurement of the inclusive and differential t(t)over-bar gamma cross sections in the dilepton channel and effective field theory interpretation in proton-proton collisions at root s=13 TeV"

Tumasyan, A.; Adam, W.; Andrejkovic, J. W.; **Chinellato, J. A.***; et al. CMS Collaboration

The production cross section of a top quark pair in association with a photon is measured in proton-proton collisions in the decay channel with two oppositely charged leptons (e(+/-)mu(-/+), e(+)e(-), or mu(+)mu(-)). The measurement is performed using 138 fb(-1) of proton-proton collision data recorded by the CMS experiment at root s = 13 TeV during the 2016-2018 data-taking period of the CERN LHC. A fiducial phase space is defined such that photons radiated by initial-state particles, top quarks, or any of their decay products are included. An inclusive cross section of 175.2 +/- 2.5(stat) +/- 6.3(syst) fb is measured in a signal region with at least one jet coming from the hadronization of a bottom quark and exactly one photon with transverse momentum above 20 GeV. Differential cross sections are measured as functions of several kinematic observables of the photon, leptons, and jets, and compared to standard model predictions. The measurements are also interpreted in the standard model effective field theory framework, and limits are found on the relevant Wilson coefficients from these results alone and in combination with a previous CMS measurement of the t (t) over bar gamma production process using the lepton+jets final state.

JOURNAL OF HIGH ENERGY PHYSICS [5], 091, 2022. DOI: 10.1007/JHEP05(2022)091

[P103-2022] "Measurement of the inclusive t(t)over-bar production cross section in proton-proton collisions at root s=5.02 TeV"

Tumasyan, A.; Adam, W.; Andrejkovic, J. W.; **Chinellato, J. A.***; et al. CMS Collaboration

The top quark pair production cross section is measured in proton-proton collisions at a center-of-mass energy of 5.02 TeV.The data were collected in a special LHC low-energy and low-intensity run in 2017, and correspond to an integrated luminosity of 302 pb(-1). The measurement is performed using events with one electron and one muon of opposite charge, and at least two jets. The measured cross section is 60.7 +/- 5.0 (stat) +/- 2.8 (syst) +/- 1.1 (lumi) pb. A combination with the result in the single lepton + jets channel, based on data collected in 2015 at the same center-of-mass energy and corresponding to an integrated luminosity of 27.4 pb(-1), is then performed. The resulting measured value is 63.0 +/- 4.1 (stat) +/- 3.0 (syst+lumi) pb, in agreement with the standard model prediction of 66.8(-3.1)(+2.9) pb.

JOURNAL OF HIGH ENERGY PHYSICS 4, 144, 2022. DOI: 10.1007/jhepo4(2022)144

[P104-2022] "Measurements of the groomed and ungroomed jet angularities in pp collisions at root s=5.02 TeV"

Acharya, S.; Adamova, D.; Adler, A.; **Chinellato, D. D.*; Guardiano, G. G.*; Jahnke, C.*; Takahashi, J.***; et al. ALICE Collaboration

The jet angularities are a class of jet substructure observables which characterize the angular and momentum distribution of particles within jets. These observables are sensitive to momentum scales ranging from perturbative hard scatterings to nonperturbative fragmentation into final-state hadrons. We report measurements of several groomed and ungroomed jet angularities in pp collisions at root s = 5.02 TeV with the ALICE detector. Jets are reconstructed using charged particle tracks at midrapidity (vertical bar eta vertical bar< 0.9). The anti-k(T) algorithm is used with jet resolution parameters R = 0.2 and R = 0.4 for several transverse momentum p(T)(ch jet) intervals in the 20-100 GeV/c range. Using the jet grooming algorithm Soft Drop, the sensitivity to softer, wide-angle processes, as well as the underlying event, can be reduced in a way which is well-controlled in theoretical calculations. We report the ungroomed jet angularities, lambda(alpha), and groomed jet angularities, lambda(alpha,g), to investigate the interplay between perturbative and nonperturbative effects at low jet momenta. Various angular exponent parameters alpha = 1, 1.5, 2, and 3 are used to systematically vary the sensitivity of the observable to collinear and soft radiation. Results are compared to analytical predictions at next-to-leading-logarithmic accuracy, which provide a generally good description of the data in the perturbative regime but exhibit discrepancies in the nonperturbative regime. Moreover, these measurements serve as a baseline for future ones in heavy-ion collisions by providing new insight into the interplay between perturbative and nonperturbative effects in the angular and momentum substructure of jets. They supply crucial guidance on the selection of jet resolution parameter, jet transverse momentum, and angular scaling variable for jet quenching studies.

JOURNAL OF HIGH ENERGY PHYSICS [5], 061, 2022. DOI: 10.1007/JHEPO5(2022)061

[P105-2022] "Neurophotonic tools for microscopic measurements and manipulation: status report"

Abdelfattah, A. S.; Ahuja, S.; Akkin, T.; **Mesquita, R. C.***; et al.

Neurophotonics was launched in 2014 coinciding with the launch of the BRAIN Initiative focused on development of technologies for advancement of neuroscience. For the last seven years, Neurophotonics' agenda has been well aligned with this focus on neurotechnologies featuring new optical methods and tools applicable to brain studies. While the BRAIN Initiative 2.0 is pivoting towards applications of these novel tools in the quest to understand the brain, this status report reviews an extensive and diverse toolkit of novel methods to explore brain function that have emerged from the BRAIN Initiative and related large-scale efforts for measurement and manipulation of brain structure and function.

Here, we focus on neurophotonic tools mostly applicable to animal studies. A companion report, scheduled to appear later this year, will cover diffuse optical imaging methods applicable to noninvasive human studies. For each domain, we outline the current state-of-the-art of the respective technologies, identify the areas where innovation is needed, and provide an outlook for the future directions.

NEUROPHOTONICS 9, 013001, Suplemento 1, 2022. DOI: 10.1117/1.NPh.9.S1.013001

[P106-2022] "Neutrino-(anti)neutrino forward scattering potential for massive neutrinos at low energies"

Dedin Neto, P.*; Kemp, E.*

In this work, we calculate the expression for the potential due to neutrino-(anti)neutrino forward scattering at low energies (E << m(Z0)) for ultra-relativistic massive neutrinos (E >> m nu), a representative regime within astrophysical scenarios. There is a broadly used expression for this potential in the literature, which, however, lacks an explicit derivation from basic principles of quantum field theory. Therefore, this paper has an intention to guide the reader through the steps and concepts to derive this potential, trying to be clear and pedagogical. Moreover, we used a rigorous approach concerning the massive nature of the neutrinos, using massive quantized neutrino fields throughout the entire process, while the usual approach is to consider massless neutrino fields at the interaction. In this context, we explicitly show the validity of the massless neutrino fields approximation at the ultra-relativistic regime, as expected. As the last step, we connect the potential expression to the density matrix formalism, which is a usual framework for works considering neutrino-neutrino interactions. We also discuss some theoretical details through the paper such as the normal ordering of quantum operators and the implications of massive fields in the neutrino state at its production.

MODERN PHYSICS LETTERS A 37[08], 2250048, 2022. DOI: 10.1142/S0217732322500481

[P107-2022] "Non-equilibrium free-energy calculation of phase-boundaries using LAMMPS"

Cajahuaringa, S.*; Antonelli, A.*

We present a guide to compute the phase-boundaries of classical systems using a dynamic Clausius-Clapeyron integration (dCCI) method within the LAMMPS (Large-scale Atomic/Molecular Massively Parallel Simulator) code. The advantage of the dCCI method is because it provides coexistence curves spanning a wide range of thermodynamic states using relatively short single non-equilibrium simulations. We describe the state-of-the-art of non-equilibrium free-energy methods that allow us to compute the Gibbs free-energy in a wide interval of pressure and/or temperature. We present the dCCI method in details, discuss its implementation in the LAMMPS package and make available source code, scripts, as well as auxiliary files. As an illustrative example, we determine the phase diagram of silicon in a range of pressures covering from 0 to 15 GPa and temperatures as low as 400 K up to the liquid phase, in order to obtain the phase boundaries and triple point between diamond, liquid and beta-Sn phases.

COMPUTATIONAL MATERIALS SCIENCE 207, 111275, 2022. DOI: 10.1016/j.commatsci.2022.111275

[P108-2022] "Production of light (anti)nuclei in pp collisions at root s=5.02 TeV"

Acharya, S.; Adamova, D.; Adler, A.; **Chinellato, D. D.*; Guardiano, G. G.*; Jahnke, C.*; Takahashi, J.*;** et al. ALICE Collaboration

The study of the production of nuclei and antinuclei in pp collisions has proven to be a powerful tool to investigate the formation mechanism of loosely bound states in high-energy hadronic collisions. In this paper, the production of protons, deuterons and He-3 and their charge conjugates at midrapidity is studied as a function of the charged-particle multiplicity in inelastic pp collisions at root s = 5.02 TeV using the ALICE detector. Within the uncertainties, the yields of nuclei in pp collisions at root s = 5.02 TeV are compatible with those in pp collisions at different energies and to those in p-Pb collisions when compared at similar multiplicities. The measurements are compared with the expectations of coalescence and Statistical Hadronisation Models. The results suggest a common formation mechanism behind the production of light nuclei in hadronic interactions and confirm that they do not depend on the collision energy but on the number of produced particles.

EUROPEAN PHYSICAL JOURNAL C 82[4], 289, 2022. DOI: 10.1140/epjc/s10052-022-10241-z

[P109-2022] "Prompt and non-prompt J/psi production cross sections at midrapidity in proton-proton collisions at root s=5.02 and 13 TeV"

Acharya, S.; Adamova, D.; Adler, A.; **Chinellato, D. D.*; Guardiano, G. G.*; Jahnke, C.*; Takahashi, J.***; et al. ALICE Collaboration

The production of J/psi is measured at midrapidity (vertical bar y vertical bar < 0.9) in proton-proton collisions at root s = 5.02 and 13 TeV, through the dielectron decay channel, using the ALICE detector at the Large Hadron Collider. The data sets used for the analyses correspond to integrated luminosities of L-int = 19.4 +/- 0.4 nb(-1)and L-int = 32.2 +/- 0.5 nb(-1) at root s = 5.02 and 13 TeV, respectively. The fraction of non-prompt J/psi mesons, i.e. those originating from the decay of beauty hadrons, is measured down to a transverse momentum p(T) = 2 GeV/c (1GeV/c) at root s = 5.02 TeV (13 TeV). The p(T) and rapidity (y) differential cross sections, as well as the corresponding values integrated over p(T) and y, are carried out separately for prompt and non-prompt J/psi mesons. The results are compared with measurements from other experiments and theoretical calculations based on quantum chromodynamics (QCD). The shapes of the p(T) and y distributions of beauty quarks predicted by state-of-the-art perturbative QCD models are used to extrapolate an estimate of the b (b) over bar pair cross section at midrapidity and in the total phase space. The total b (b) over bar cross sections are found to be sigma(b (b) over bar) = 541 +/- 45 (stat.) +/- 69 (syst.)(-12)(+10) (extr.) mu b and sigma(b (b) over bar) = 218 +/- 37 (stat.)+/- 31 (syst.) (-9.1)(+8.2) (extr.) mu b at root s = 13 and 5.02 TeV, respectively. The value obtained from the combination of ALICE and LHCb measurements in pp collisions at root s = 13 TeV is also provided.

JOURNAL OF HIGH ENERGY PHYSICS [3], 190, 2022. DOI: 10.1007/JHEP03(2022)190

[P110-2022] "Quantum entanglement in a four-partite hybrid system containing three macroscopic subsystems"

Correa Jr., C.*; Vidiella-Barranco, A.*

In this work, we consider a setup consisting of an atomic ensemble enclosed within a laser-driven optomechanical cavity, having the moving mirror further (capacitively) coupled to a low-frequency LC circuit. This constitutes a four-partite optoelectromechanical quantum system containing three macroscopic quantum subsystems of a different nature, viz, the atomic ensemble, the massive mirror and the LC circuit.

The quantized cavity field plays the role of an auxiliary system that allows the coupling of two other quantum subsystems. We show that for experimentally achievable parameters, it is possible to generate steady-state bipartite Gaussian entanglement between pairs of macroscopic systems. In particular, we find under which conditions it is possible to obtain a reasonable amount of entanglement between the atomic ensemble and the LC circuit, systems that might be suitable for constituting a quantum memory and for quantum processing, respectively. For complementarity, we discuss the effect of the environmental temperature on quantum entanglement.

EUROPEAN PHYSICAL JOURNAL PLUS 137[4], 473, 2022. DOI: 10.1140/epjp/s13360-022-02696-6

[P111-2022] "Revealing the impact of strain in the optical properties of bubbles in monolayer MoSe2"

Covre, F. S.; Faria Jr., P. E.; **Gordo, V. O.*;** Brito, C. S. de; Zhumagulov, Y., V; Teodoro, M. D.; **Couto Jr., O. D. D.*;** Misoguti, L.; Pratavieira, S.; Andrade, M. B.; Christianen, P. C. M.; Fabian, J.; Withers, F.; Gobato, Y. G.

Strain plays an important role for the optical properties of monolayer transition metal dichalcogenides (TMDCs). Here, we investigate strain effects in a monolayer MoSe2 sample with a large bubble region using mu-Raman, second harmonic generation (SHG), mu-photoluminescence and magneto mu-photoluminescence at low temperature. Remarkably, our results reveal the presence of a non-uniform strain field and the observation of emission peaks at lower energies which are the signatures of exciton and trion quasiparticles red-shifted by strain effects in the bubble region, in agreement with our theoretical predictions. Furthermore, we have observed that the emission in the strained region decreases the trion binding energy and enhances the valley g-factors as compared to non-strained regions. Considering uniform biaxial strain effects within the unit cell of the TMDC monolayer (ML), our first principles calculations predict the observed enhancement of the exciton valley Zeeman effect. In addition, our results suggest that the exciton--trion fine structure plays an important role for the optical properties of strained TMDC ML. In summary, our study provides fundamental insights on the behaviour of excitons and trions in strained monolayer MoSe2 which are particularly relevant to properly characterize and understand the fine structure of excitonic complexes in strained TMDC systems/devices.

NANOSCALE 14[15], 5758-5768, 2022. DOI: 10.1039/d2nr00315e

[P112-2022] "Search for a heavy resonance decaying into a top quark and a W boson in the lepton plus jets final state at root s=13 TeV"

Tumasyan, A.; Adam, W.; Andrejkovic, J. W.; **Chinellato, J. A.***; et al. CMS Collaboration

A search for a heavy resonance decaying into a top quark and a W boson in proton-proton collisions at root s = 13TeV is presented. The data analyzed were recorded with the CMS detector at the LHC and correspond to an integrated luminosity of 138 fb(-1). The top quark is reconstructed as a single jet and the W boson, from its decay into an electron or muon and the corresponding neutrino. A top quark tagging technique based on jet clustering with a variable distance parameter and simultaneous jet grooming is used to identify jets from the collimated top quark decay. The results are interpreted in the context of two benchmark models, where the heavy resonance is either an excited bottom quark b* or a vector-like quark B. A statistical combination with an earlier search by the CMS Collaboration in the all--hadronic final state is performed to place upper cross section limits on these two models. The new analysis extends the lower range of resonance mass probed from 1.4 down to 0.7TeV. For left-handed, right-handed, and vector-like couplings, b* masses up to 3.0, 3.0, and 3.2TeV are excluded at 95% confidence level, respectively. The observed upper limits represent the most stringent constraints on the b* model to date.

JOURNAL OF HIGH ENERGY PHYSICS [4], 048, 2022. DOI: 10.1007/JHEP04(2022)048

[P113-2022] "Search for a right-handed W boson and a heavy neutrino in proton-proton collisions at root s=13 TeV"

Tumasyan, A.; Adam, W.; Andrejkovic, J. W.; **Chinellato, J. A.***; et al. CMS Collaboration

A search is presented for a right-handed W boson (W-R) and a heavy neutrino (N), in a final state consisting of two same-flavor leptons (ee or mu mu) and two quarks. The search is performed with the CMS experiment at the CERN LHC using a data sample of proton-proton collisions at a center-of-mass energy of 13TeV corresponding to an integrated luminosity of 138 fb(-1). The search covers two regions of phase space, one where the decay products of the heavy neutrino are merged into a single large-area jet, and one where the decay products are well separated. The expected signal is characterized by an excess in the invariant mass distribution of the final-state objects. No significant excess over the standard model background expectations is observed. The observations are interpreted as upper limits on the product of W-R production cross sections and branching fractions assuming that couplings are identical to those of the standard model W boson. For N masses m(N) equal to half the W-R mass m(WR) (m(N) = 0.2TeV), mW(R) is excluded at 95% confidence level up to 4.7 (4.8) and 5.0 (5.4) TeV for the electron and muon channels, respectively. This analysis provides the most stringent limits on the WR mass to date.

JOURNAL OF HIGH ENERGY PHYSICS [4], 047, 2022. DOI: 10.1007/JHEP04(2022)047

[P114-2022] "Search for electroweak production of charginos and neutralinos in proton-proton collisions at root s=13 TeV"

Tumasyan, A.; Adam, W.; Andrejkovic, J. W.; **Chinellato, J. A.***; et al. CMS Collaboration

A direct search for electroweak production of charginos and neutralinos is presented. Events with three or four leptons, with up to two hadronically decaying tau leptons, or two same-sign light leptons are analyzed. The data sample consists of 137 fb(-1) of proton-proton collisions with a center of mass energy of 13 TeV, recorded with the CMS detector at the LHC. The results are interpreted in terms of several simplified models. These represent a broad range of production and decay scenarios for charginos and neutralinos. A parametric neural network is used to target several of the models with large backgrounds. In addition, results using orthogonal search regions are provided for all the models, simplifying alternative theoretical interpretations of the results. Depending on the model hypotheses, charginos and neutralinos with masses up to values between 300 and 1450 GeV are excluded at 95% confidence level.

JOURNAL OF HIGH ENERGY PHYSICS [4], 147, 2022. DOI: 10.1007/JHEP04(2022)147

[P115-2022] "Search for heavy resonances decaying to a pair of Lorentz-boosted Higgs bosons in final states with leptons and a bottom quark pair at root s=13 TeV"

Tumasyan, A.; Adam, W.; Andrejkovic, J. W.; **Chinellato, J. A.***; et al. CMS Collaboration

A search for new heavy resonances decaying to a pair of Higgs bosons (HH) in proton-proton collisions at a center-of-mass energy of 13 TeV is presented. Data were collected with the CMS detector at the LHC in 2016-2018, corresponding to an integrated luminosity of 138 fb(-1). Resonances with a mass between 0.8 and 4.5 TeV are considered using events in which one Higgs boson decays into a bottom quark pair and the other into final states with either one or two charged leptons. Specifically, the single-lepton decay channel HH -> b (b) over bar WW* -> b (b) over bar lvq (q) over bar' and the dilepton decay channels HH -> b (b) over bar WW* -> b (b) over bar lvlv and HH -> b (b) over bar tau tau -> b (b) over bar lvvlvv are examined, where l in the final state corresponds to an electron or muon. The signal is extracted using a two--dimensional maximum likelihood fit of the H -> b (b) over bar jet mass and HH invariant mass distributions. No significant excess above the standard model expectation is observed in data. Model-independent exclusion limits are placed on the product of the cross section and branching fraction for narrow spin-0 and spin-2 massive bosons decaying to HH. The results are also interpreted in the context of radion and bulk graviton production in models with a warped extra spatial dimension. The results provide the most stringent limits to date for X -> HH signatures with final-state leptons and at some masses provide the most sensitive limits of all X -> HH searches.

JOURNAL OF HIGH ENERGY PHYSICS [5], 005, 2022. DOI: 10.1007/JHEP05(2022)005

[P116-2022] "Search for heavy resonances decaying to WW, WZ, or WH boson pairs in a final state consisting of a lepton and a large-radius jet in proton-proton collisions at root s=13 TeV"

Tumasyan, A.; Adam, W.; Andrejkovic, J. W.; **Chinellato, J. A.***; et al. CMS Collaboration

A search for new heavy resonances decaying to pairs of bosons (WW, WZ, or WH) is presented. The analysis uses data from proton-proton collisions collected with the CMS detector at a center-of-mass energy of 13 TeV, corresponding to an integrated luminosity of 137 fb(-1). One of the bosons is required to be a W boson decaying to an electron or muon and a neutrino, while the other boson is required to be reconstructed as a single jet with mass and substructure compatible with a quark pair from a W, Z, or Higgs boson decay. The search is performed in the resonance mass range between 1.0 and 4.5 TeVand includes a specific search for resonances produced via vector boson fusion. The signal is extracted using a twodimensional maximum likelihood fit to the jet mass and the diboson invariant mass distributions. No significant excess is observed above the estimated background. Model--independent upper limits on the production cross sections of spin-0, spin-1, and spin-2 heavy resonances are derived as functions of the resonance mass and are interpreted in the context of bulk radion, heavy vector triplet, and bulk graviton models. The reported bounds are the most stringent to date.

PHYSICAL REVIEW D 105[3], 032008, 2022. DOI: 10.1103/PhysRevD.105.032008

[P117-2022] "Search for heavy resonances decaying to ZZ or ZW and axion-like particles mediating nonresonant ZZ or ZH production at root s=13 TeV"

Tumasyan, A.; Adam, W.; Andrejkovic, J. W.; **Chinellato, J. A.***; et al. CMS Collaboration

A search has been performed for heavy resonances decaying to ZZ or ZW and for axion-like particles (ALPs) mediating nonresonant ZZ or ZH production, in final states with two charged leptons (l = e, mu) produced by the decay of a Z boson, and two quarks produced by the decay of a Z, W, or Higgs boson H. The analysis is sensitive to resonances with masses in the range 450 to 2000 GeV. Two categories are defined corresponding to the merged or resolved reconstruction of the hadronically decaying boson. The search is based on data collected during 2016-2018 by the CMS experiment at the LHC in proton-proton collisions at a center-of-mass energy of 13 TeV, corresponding to an integrated luminosity of 138 fb(-1). No significant excess is observed in the data above the standard model background expectation. Upper limits on the production cross section of heavy, narrow spin-2 and spin-1 resonances are derived as functions of the resonance mass, and exclusion limits on the production of bulk graviton particles and W ' bosons are calculated in the framework of the warped extra dimensions and heavy vector triplet models, respectively. In addition, upper limits on the ALP-mediated diboson production cross section and ALP couplings to standard model particles are obtained in the framework of linear and chiral effective field theories. These are the first limits on nonresonant ALP-mediated ZZ and ZH production obtained by the LHC experiments.

JOURNAL OF HIGH ENERGY PHYSICS [4], 087, 2022. DOI: 10.1007/JHEP04(2022)087

[P118-2022] "Search for higgsinos decaying to two Higgs bosons and missing transverse momentum in proton-proton collisions at root s=13 TeV"

Tumasyan, A.; Adam, W.; Andrejkovic, J. W.; **Chinellato, J. A.***; et al. CMS Collaboration

Results are presented from a search for physics beyond the standard model in proton-proton collisions at root s = 13 TeV in channels with two Higgs bosons, each decaying via the process H -> b (b) over bar, and large missing transverse momentum. The search uses a data sample corresponding to an integrated luminosity of 137fb(-1) collected by the CMS experiment at the CERN LHC. The search is motivated by models of supersymmetry that predict the production of neutralinos, the neutral partners of the electroweak gauge and Higgs bosons. The observed event yields in the signal regions are found to be consistent with the standard model background expectations. The results are interpreted using simplified models of supersymmetry. For the electroweak production of nearly mass-degenerate higgsinos, each of whose decay chains yields a neutralino ((chi) over tilde (0)(1)) that in turn decays to a massless goldstino and a Higgs boson, (chi) over tilde (0)(1) masses in the range 175 to 1025 GeV are excluded at 95% confidence level. For the strong production of gluino pairs decaying via a slightly lighter (chi) over tilde (0)(2) to H and a light (chi) over tilde (0)(1), gluino masses below 2330 GeV are excluded.

JOURNAL OF HIGH ENERGY PHYSICS [5], 014, 2022. DOI: 10.1007/JHEP05(2022)014

[P119-2022] "Search for long-lived particles decaying into muon pairs in proton-proton collisions at root s=13 TeV collected with a dedicated high-rate data stream"

Tumasyan, A.; Adam, W.; Andrejkovic, J. W.; **Chinellato, J. A.*;** et al. CMS Collaboration

A search for long-lived particles decaying into muon pairs is performed using proton-proton collisions at a center-of-mass energy of 13 TeV, collected by the CMS experiment at the LHC in 2017 and 2018, corresponding to an integrated luminosity of 101 fb(-1). The data sets used in this search were collected with a dedicated dimuon trigger stream with low transverse momentum thresholds, recorded at high rate by retaining a reduced amount of information, in order to explore otherwise inaccessible phase space at low dimuon mass and nonzero displacement from the primary interaction vertex.

No significant excess of events beyond the standard model expectation is found. Upper limits on branching fractions at 95% confidence level are set on a wide range of mass and lifetime hypotheses in beyond the standard model frameworks with the Higgs boson decaying into a pair of long-lived dark photons, or with a long-lived scalar resonance arising from a decay of a b hadron. The limits are the most stringent to date for substantial regions of the parameter space. These results can be also used to constrain models of displaced dimuons that are not explicitly considered in this paper.

JOURNAL OF HIGH ENERGY PHYSICS [4], 062, 2022. DOI: 10.1007/JHEP04(2022)062

[P120-2022] "Search for long-lived particles produced in association with a Z boson in proton-proton collisions at root s=13 TeV"

Tumasyan, A.; Adam, W.; Andrejkovic, J. W.; **Chinellato, J. A.***; et al. CMS Collaboration

A search for long-lived particles (LLPs) produced in association with a Z boson is presented. The study is performed using data from proton-proton collisions with a center-of-mass energy of 13 TeV recorded by the CMS experiment during 2016-2018, corresponding to an integrated luminosity of 117fb(-1).( )The LLPs are assumed to decay to a pair of standard model quarks that are identified as displaced jets within the CMS tracker system. Triggers and selections based on Z boson decays to electron or muon pairs improve the sensitivity to light LLPs (down to 15 GeV). This search provides sensitivity to beyond the standard model scenarios which predict LLPs produced in association with a Z boson. In particular, the results are interpreted in the context of exotic decays of the Higgs boson to a pair of scalar LLPs (H -> SS). The Higgs boson decay branching fraction is constrained to values less than 6% for proper decay lengths of 10-100 mm and for LLP masses between 40 and 55 GeV. In the case of low-mass (approximate to 15 GeV) scalar particles that subsequently decay to a pair of b quarks, the search is sensitive to branching fractions B(H -> SS) < 20% for proper decay lengths of 10-50 mm. The use of associated production with a Z boson increases the sensitivity to low-mass LLPs of this analysis with respect to gluon fusion searches. In the case of 15 GeV scalar LLPs, the improvement corresponds to a factor of 2 at a proper decay length of 30 mm.

JOURNAL OF HIGH ENERGY PHYSICS [3], 160, 2022. DOI: 10.1007/JHEP03(2022)160

[P121-2022] "Search for low-mass dilepton resonances in Higgs boson decays to four-lepton final states in proton-proton collisions at root s=13 TeV"

Tumasyan, A.; Adam, W.; Bergauer, T.; **Chinellato, J. A.***; et al. CMS Collaboration

A search for low-mass dilepton resonances in Higgs boson decays is conducted in the four-lepton final state. The decay is assumed to proceed via a pair of beyond the standard model particles, or one such particle and a Z boson. The search uses proton-proton collision data collected with the CMS detector at the CERN LHC, corresponding to an integrated luminosity of 137 fb(-1), at a center-of-mass energy root s = 13 TeV. No significant deviation from the standard model expectation is observed. Upper limits at 95% confidence level are set on model-independent Higgs boson decay branching fractions. Additionally, limits on dark photon and axion-like particle production, based on two specific models, are reported.

EUROPEAN PHYSICAL JOURNAL C 82[4], 290, 2022. DOI: 10.1140/epjc/s10052-022-10127-0

[P122-2022] "Search for single production of a vector-like T quark decaying to a top quark and a Z boson in the final state with jets and missing transverse momentum at root s=13 TeV"

Tumasyan, A.; Adam, W.; Andrejkovic, J. W.; **Chinellato, J. A.*;** et al. CMS Collaboration

A search is presented for single production of a vector-like T quark with charge 2/3 e, in the decay channel featuring a top quark and a Z boson, with the top quark decaying hadronically and the Z boson decaying to neutrinos. The search uses data collected by the CMS experiment in proton-proton collisions at a center-of-mass energy of 13 TeV, corresponding to an integrated luminosity of 137 fb(-1) recorded at the CERN LHC in 2016-2018. The search is sensitive to a T quark mass between 0.6 and 1.8 TeV with decay widths ranging from negligibly small up to 30% of the T quark mass. Reconstruction strategies for the top quark are based on the degree of Lorentz boosting of its final state. At 95% confidence level, the upper limit on the product of the cross section and branching fraction for a T quark of small decay width varies between 15 and 602 fb, depending on its mass. For a T quark with decay widths between 10 and 30% of its mass, this upper limit ranges between 16 and 836 fb. For most of the studied range, the results provide the best limits to date. This is the first search for single T quark production based on the full Run 2 data set of the LHC.

JOURNAL OF HIGH ENERGY PHYSICS [5], 093, 2022. DOI: 10.1007/JHEP05(2022)093

[P123-2022] "Search for supersymmetry in final states with two or three soft leptons and missing transverse momentum in proton-proton collisions at root s=13 TeV"

Tumasyan, A.; Adam, W.; Andrejkovic, J. W.; **Chinellato, J. A.***; et al. CMS Collaboration

A search for supersymmetry in events with two or three low--momentum leptons and missing transverse momentum is performed. The search uses proton-proton collisions at root s = 13TeV collected in the three-year period 2016-2018 by the CMS experiment at the LHC and corresponding to an integrated luminosity of up to 137 fb(-1). The data are found to be in agreement with expectations from standard model processes. The results are interpreted in terms of electroweakino and top squark pair production with a small mass difference between the produced supersymmetric particles and the lightest neutralino. For the electroweakino interpretation, two simplified models are used, a wino-bino model and a higgsino model. Exclusion limits at 95% confidence level are set on (X) over tilde (0)(2) /(X) over tilde (+/-)(1) masses up to 275 GeV for a mass difference of 10 GeV in the wino-bino case, and up to 205(150) GeV for a mass difference of 7.5 (3) GeV in the higgsino case. The results for the higgsino are further interpreted using a phenomenological minimal supersymmetric standard model, excluding the higgsino mass parameter mu up to 180 GeV with the bino mass parameter M-1 at 800 GeV. In the top squark interpretation, exclusion limits are set at top squark masses up to 540 GeV for four-body top squark decays and up to 480 GeV for chargino-mediated decays with a mass difference of 30 GeV.

JOURNAL OF HIGH ENERGY PHYSICS [4], 091, 2022. DOI: 10.1007/JHEP04(2022)091

[P124-2022] "Search for W? resonances in proton-proton collisions at vs=13 TeV using hadronic decays of Lorentz--boosted W bosons"

Tumasyan, A.; Adam, W.; Andrejkovic, J. W.; **Chinellato, J. A.***; et al. CMS Collaboration

A search for W gamma resonances in the mass range between 0.7 and 6.0 TeV is presented. The W boson is reconstructed via its hadronic decays, with the final-state products forming a single large-radius jet, owing to a high Lorentz boost of the W boson. The search is based on proton-proton collision data at root s = 13 TeV, corresponding to an integrated luminosity of 137 fb(-1), collected with the CMS detector at the LHC in 2016-2018. The W gamma mass spectrum is parameterized with a smoothly falling background function and examined for the presence of resonance-like signals. No significant excess above the predicted background is observed. Model-specific upper limits at 95% confidence level on the product of the cross section and branching fraction to the W gamma channel are set. Limits for narrow resonances and for resonances with an intrinsic width equal to 5% of their mass, for spin-0 and spin-1 hypotheses, range between 0.17 fb at 6.0 TeV and 55 fb at 0.7 TeV. These are the most restrictive limits to date on the existence of such resonances over a large range of probed masses. In specific heavy scalar (vector) triplet benchmark models, narrow resonances with masses between 0.75 (1.15) and 1.40 (1.36) TeV are excluded for a range of model parameters. Model-independent limits on the product of the cross section, signal acceptance, and branching fraction to the W gamma channel are set for minimum W gamma mass thresholds between 1.5 and 8.0 TeV.

PHYSICS LETTERS B 826, 136888, 2022. DOI: 10.1016/j.physletb.2022.136888

[P125-2022] "Spin alignment of vector mesons as a probe of spin hydrodynamics and freeze-out"

Goncalves, K. J.*; Torrieri, G.*

We argue that a detailed analysis of the spin alignment of vector mesons can serve as a probe of two little understood aspects of spin dynamics in a vortical fluid: The degree of relaxation between vorticity and particle spin polarization, and the degree of coherence of the hadron wave function at freeze-out. We illustrate these with a coalescence model.

PHYSICAL REVIEW C 105[3], 034913, 2022. DOI: 10.1103/PhysRevC.105.034913

[P126-2022] "Study of dijet events with large rapidity separation in proton-proton collisions at root s=2.76 TeV"

Tumasyan, A.; Adam, W.; Andrejkovic, J. W.; **Chinellato, J. A.***; et al. CMS Collaboration

The cross sections for inclusive and Mueller-Navelet dijet production are measured as a function of the rapidity separation between the jets in proton-proton collisions at root s = 2.76 TeV for jets with transverse momentum p(T) > 35 GeV and rapidity vertical bar y vertical bar < 4.7. Various dijet production cross section ratios are also measured. A veto on additional jets with p(T) > 20 GeV is introduced to improve the sensitivity to the effects of the Balitsky-Fadin-Kuraev-Lipatov (BFKL) evolution. The measurement is compared with the predictions of various Monte Carlo models based on leading-order and next-to-leading-order calculations including the Dokshitzer-Gribov-Lipatov-Altarelli-Parisi leading-logarithm (LL) parton shower as well as the LL BFKL resummation.

JOURNAL OF HIGH ENERGY PHYSICS [3], 189, 2022. DOI: 10.1007/JHEP03(2022)189

[P127-2022] "Temperature and entanglement of the three--state quantum walk"

Tude, L. T.*; Oliveira, M. C. de*

In the present work, the evolution of a three state quantum walk without decoherence is investigated. Despite being a closed quantum system under unitary evolution, its Hilbert space can be divided in two subspaces, which enables the analysis of the subsystems (the coin or the walker) as an open system in contact with a reservoir. We calculate the asymptotic reduced density matrix of the coin space of the three-state quantum walk in an infinite line, and use that result to analyze the entanglement between the chirality, and position space. We calculate the von Neumann entropy and the entanglement temperature per mean energy of the system in the asymptotic limit.

QUANTUM SCIENCE AND TECHNOLOGY 7[3], 035009, 2022. DOI: 10.1088/2058-9565/ac6a05

[P128-2022] "Temperature estimation of a pair of trapped ions"

Sa Neto, O. P. de; Costa, H. A. S.; Prataviera, G. A.; **Oliveira, M. C. de***

We apply estimation theory to a system formed by two interacting trapped ions. By using the Fisher matrix formalism, we introduce a simple scheme for estimation of the temperature of the longitudinal vibrational modes of the ions. We use the ions interaction to effectively infer the temperature of the individual ions, by optimising the interaction time evolution and by measuring only over one of the ions. We also investigate the effect of a non-thermal reservoir over the inference approach. The non-classicality of one of the ions vibrational modes, introduced due to a squeezed thermal reservoir, does not directly affect the inference of the individual temperatures, although allowing the modes to be entangled. To check actual experimental conditions, we analyze the temperature inference under heating due to surface-electrode noise.

SCIENTIFIC REPORTS 12[1], 6697, 2022. DOI: 10.1038/s41598-022-10572-7

[P129-2022] "The effect of plasma treatment on flexible self-standing supercapacitors composed by carbon nanotubes and multilayer graphene composites"

Moreto, J. A.; Silva, P. H. S.; Moura, G. D. de; Silva, C. C. da; Ferreira, D. C.; Cunha, T. H. R. da; Silva, G. G.; **Rouxinol, F.*; Siervo, A. de*;** Gelamo, R. V.

Flexible self-standing supercapacitor devices (FSSS) have attracted great attention in several areas due to their potential use in a wide range of applications, such as roll-up displays, wearable electronics, and storage energy devices. However, the success of FSSS devices is highly dependent on their electrochemical properties. Here, we presented an innovative process for the preparation of novel low-cost ionic gel and superficial CO2 plasma treatment to modify electrodes based on multiwall carbon nanotubes (MWCNT) and multilayer graphene (MLG). The hybrid supercapacitors were characterized morphologically and structurally via scanning electron microscopy, atomic force microscopy, Raman spectroscopy, and X-ray photoelectron spectroscopy. To assess the electrochemical properties, cyclic voltammetry, galvanostatic charge-discharge, and electrochemical impedance spectroscopy were used. The morphological results showed that the new CO2 plasma treatment promoted a better distribution of the carbon components, improving the contact area between the electrolyte and the electrode surface. Electrochemical tests demonstrated excellent behavior of the electrolyte gel, with specific capacitances of 256 mF cm(-2) and 603 F g(-1), energy and power densities of 24.03 mu Wh cm(-2) and 2.16 mW cm(-2), respectively.

Additionally, the CNT incorporation on the MLG electrodes and the plasma treatment were important factors to produce flexible supercapacitors fashion. The MLG + MWCNT pure and plasma treated appeared as remarkable material for flexible high-performance energy storage devices.

JOURNAL OF MATERIALS SCIENCE 57[19], 8779-8799, 2022. DOI: 10.1007/s10853-022-07162-3

[P130-2022] "Triphenylboroxine stability under low-energy-electron interactions"

Pereira-da-Silva, J.; Mendes, M.; Nunes, A.; Araujo, J.; **Cornetta, L.***; Silva, F. F. da

Triphenylboroxine (TPB) has chemical properties of great interest in organic synthesis, enabling the development of promising molecular architectures. Based on the possibility of the geometric arrangement of N-coordinated boron atoms, the dynamic interconversion ability of boroxine cages enables the optimization of relevant pharmacological properties in drug delivery, such as guest recognition and porosity. In addition, the synthesis of a novel 2D boroxine framework showed distinctive electronic and morphological properties that can be used in the design of new electronic devices. In the present study, the electron-driven fragmentation pathways from electron interactions with TPB using a gas-phase crossed-beam experiment have been investigated. The abundance of the molecular parent cation in the mass spectrum at 70 eV reflects the stability of TPB. The appearance energies of three fragment cations were reported, and the experimental first ionization potential was found at 9.12 +/- 0.10 eV. Only the parent cation is formed in the energy range (similar to 9-16 eV) between the first ionization potential and the remaining thresholds. Regarding negative ion formation, four low-abundant anions in the electron energy range of 0-15 eV are discussed. These results indicate an interesting energy selectivity and stability of TPB upon electron interaction, which may justify the development of recent molecular architectures containing TPB used in a wide range of applications. These results are supported by quantum chemical calculations based on bound state techniques, electron ionization models and thermodynamic thresholds.

PHYSICAL CHEMISTRY CHEMICAL PHYSICS 24[17], 10025-10032 DOI: 10.1039/d2cp00855f

[P131-2022] "Tuning isolated zero-field skyrmions and spin spirals at room-temperature in synthetic ferrimagnetic multilayers"

Brandao, J.; Dugato, D. A.; **Santos, M. V. P. dos*; Beron, F.***; Cezar, J. C.

We demonstrate the observation of spin spirals and individual skyrmions in synthetic Pt/CoGd/Pt ferrimagnetic multilayers at room-temperature without the assistance of an external magnetic field. The magnetic coupling between the magnetic moments of Co and Gd, was investigated across various CoGd thicknesses by element specific X-ray magnetic circular dichroism (XMCD) performed around the Co L-2,L-3 and Gd M(4,5)edges. It show s an uncompensated ferrimagnetic orientation between the Co and Gd atoms preserved at ambient conditions, even for sub-nanometer thick layers. In addition, with the tunable enhanced perpendicular magnetic anisotropy K-u and remnant magnetization M-R found for thinner CoGd & LE; (0.9 nm) isolated zero-field skyrmions were imaged by magnetic force microscopy (MFM) as the magnetic ground state, replacing the spin spirals observed for thicker CoGd layers & GE; (1.2 nm). Such stable skyrmions in perpendicularly magnetized materials with antiparallel exchange-coupling are potential candidates for energy-efficient data storage and processing in future antiferromagnetic-based devices.

APPLIED SURFACE SCIENCE 585, 152598, 2022. DOI: 10.1016/j.apsusc.2022.152598

[P132-2022] "Two-dimensional cobalt telluride as a piezo--tribogenerator"

Negedu, S. D.; **Tromer, R.***; Gowda, C. C.; Woellner, C. F.; Olu, F. E.; Roy, A. K.; Pandey, P.; **Galvao, D. S.***; Ajayan, P. M.; Kumbhakar, P.; Tiwary, C. S.

Two-dimensional (2D) materials have been shown to be efficient in energy harvesting. Here, we report the use of waste heat to generate electricity via the combined piezoelectric and triboelectric properties of 2D cobalt telluride (CoTe2). The piezo--triboelectric nanogenerator (PTNG) produced an open-circuit voltage of similar to 5 V under 1 N force and the effect of temperature in the range of 305-363 K shows a four-fold energy conversion efficiency improvement. The 2D piezo-tribogenerator shows excellent characteristics with a maximum voltage of similar to 10 V, fast response time, and high responsivity. Density functional theory was used to gain further insights and validation of the experimental results. Our results could lead to energy harvesting approaches using 2D materials from various thermal sources and dissipating waste heat from electronic devices.

NANOSCALE, Acesso antecipado: março de 2022. DOI: 10.1039/d2nr00132b

[P133-2022] "Using Z Boson Events to Study Parton-Medium Interactions in Pb-Pb Collisions"

Sirunyan, A. M.; Tumasyan, A.; Adam, W.; **Chinellato, J. A.***; et al. CMS Collaboration

The spectra measurements of charged hadrons produced in the shower of a parton originating in the same hard scattering with a leptonically decaying Z boson arc reported in lead-lead nuclei (Pb-Pb) and proton-proton (pp) collisions at a nucleon--nucleon center-of-mass energy of 5.02 TeV. Both Pb-Pb and pp data sets are recorded by the CMS experiment at the LHC and correspond to an integrated luminosity of 1.7 nb(-1) and 320 pb(-1), respectively. Hadronic collision data with one reconstructed Z boson candidate with the transverse momentum p(T) > 30 GeV/c are analyzed. The Z boson constrains the initial energy and direction of the associated parton. In heavy ion events, azimuthal angular distributions of charged hadrons with respect to the direction of a Z boson are sensitive to modifications of the in-medium parton shower and medium response. compared to reference data from pp interactions, the results for central Pb-Pb collisions indicate a modification of the angular correlations. The measurements of the fragmentation functions and p(T) spectra of charged particles in Z boson events, which are sensitive to medium modifications of the parton shower longitudinal structure, are also reported. Significant modifications in central Pb-Pb events compared to the pp reference data are also found for these observables.

PHYSICAL REVIEW LETTERS 128[12], 122301, 2022. DOI: 10.1103/PhysRevLett.128.122301

Correções

[Co003-2022] "Measurement of exclusive Upsilon photoproduction from protons in pPb collisions at root s(NN) = 5.02 TeV (vol 79, 277, 2019)"

Sirunyan, A. M.; Tumasyan, A.; Adam, W.; **Chinellato, J. A.***; **Manganote, E. J. T.***; et al. CMS Collaboration

EUROPEAN PHYSICAL JOURNAL C 82[4], 343, 2022. DOI: 10.1140/epjc/s10052-022-10276-2

[Co004-2022] "Search for new physics in dijet angular distributions using proton-proton collisions at root s = 13TeV and constraints on dark matter and other models (vol 78, 789, 2018)"

Sirunyan, A. M.; Tumasyan, A.; Adam, W.; **Chinellato, J. A.*; Manganote, E. J. T.***; et al. CMS Collaboration

EUROPEAN PHYSICAL JOURNAL C 82[4], 379, 2022. DOI: 10.1140/epjc/s10052-022-10278-0

***Autores da comunidade IFGW**
Fonte: Web of Science on-line (WOS)

Defesas de Dissertações do IFGW

[D006-2022] "Estudo sobre a formação do estado eletreto em MoO2 pela introdução de vacâncias"
Aluno: Felipe Martins Silva
Orientador: Prof. Dr. Douglas Soares Galvão
Data: 25/04/2022

[D007-2022] "Revelando a Estrutura Fina de Nanocristais Semicondutores por Espectroscopia Coerente Multidimensional"
Aluno: Tomás Aguiar Carneiro Ferreira
Orientador: Prof. Dr. Lázaro Aurélio Padilha Júnior
Data: 11/05/2022

[D008-2022] "A estrutura de polos no vértice ghost-gluon e o mecanismo de Schwinger na QCD"
Aluno: Leonardo Rodrigues dos Santos
Orientador: Profa. Dra. Arlene Cristina Aguilar
Data: 13/05/2022

[D009-2022] "Características estruturais e propriedades ópticas de filmes finos nanocristalinos de h-BN"
Aluno: Saron Rosy Sales de Mello
Orientador: Prof. Dr. Fernando Alvarez
Data: 18/05/2022

[D010-2022] "Modulação acústica da dinâmica excitônica em monocamadas de dicalcogenetos de metais de transição"
Aluno: Diego Scolfaro da Silva
Orientador: Prof. Dr. Odilon Divino Damasceno Couto Junior
Data: 24/06/2022

[D011-2022] "Espectroscopia Raman em óxidos magnéticos com estruturas do tipo perovskita e olivina"
Aluno: Danilo Rigitano Gomes da Silva
Orientador: Prof. Dr. Eduardo Granado Monteiro da Silva
Data: 01/07/2022

[D012-2022] "Investigando as propriedades eletrônicas e ópticas de materiais atomicamente finos com um microscópio de tunelamento com varredura"
Aluno: Ricardo Javier Peña Román
Orientador: Prof. Dr. Luiz Fernando Zagonel
Data: 05/07/2022

Defesas de Teses do IFGW

[T009-2022] "Estudo de filmes nanoestruturados condutores e self-healing para aplicação em eletrônica flexível"
Aluno: Gabriel Gaal
Orientador: Prof. Dr. Varlei Rodrigues
Data: 29/04/2022

[T010-2022] "Isolantes topológico e de Chern correlacionados bidimensionais"
Aluno: Leonardo da Silva Garcia Leite
Orientador: Prof. Dr. Ricardo Luís Doretto
Data: 29/04/2022

Fonte: Portal IFGW/Pós-graduação - Agenda de Colóquios, Defesas e Seminários.
Disponível em: http://portal.ifi.unicamp.br/pos-graduacao

Abstracta

Instituto de Física
Diretor: Profa. Dra. Mônica Alonso Cotta
Diretora Associada: Prof. Dr. Marcos Cesar de Oliveira
Universidade Estadual de Campinas - UNICAMP
Cidade Universitária Zeferino Vaz
13083-859 - Campinas - SP - Brasil
e-mail: secdir@ifi.unicamp.br
Fone: +55 19 3521-5300

Publicação

Biblioteca do Instituto de Física Gleb Wataghin
http://portal.ifi.unicamp.br/biblioteca
Instagram: @bif.unicamp
Telegram: t.m/bifunicamp

Diretora Técnica: Sandra Maria Carlos Cartaxo
Coordenadora da Comissão de Biblioteca: Profa. Dra. Arlene Cristina Aguilar

Elaboração:
Maria Graciele Trevisan (Bibliotecária)
contato: infobif@ifi.unicamp.br